Field-induced nonequilibrium periodic structures in nematic liquid crystals: Nonlinear study of the twist Frederiks transition

George Srajer,* Seth Fraden,† and Robert B. Meyer
The Martin Fisher School of Physics, Brandeis University, Waltham, Massachusetts 02254
(Received 3 October 1988)

Spatially periodic structures in nematic liquid crystals usually appear as the initial response to a suddenly applied reorienting field. To account for the significant discrepancy between the measured periodicity and the periodicity calculated from a linear instability analysis we derived nonlinear equations of motion and solved them numerically. Our results agree well with the observed wavelength. We propose a novel mechanism responsible for the final wavelength selection.

During recent years much effort has been devoted to the study of pattern formation and wavelength selection in dissipative systems.[1–4] Spatially periodic structures have been observed in hydrodynamic instabilities of fluids,[5–7] crystal growth,[8] and chemical-reaction-diffusion systems,[9] just to mention a few. Reorientation instabilities in liquid crystals (LC's) belong to this class of phenomena. Although there are some differences, a major one being that in LC the instabilities are transient, detailed analysis of wavelength selection in these particular systems may contribute to a better understanding of wavelength selection in general.

When a magnetic field is applied to an initially uniformly aligned nematic LC, the average orientation axis or director $\hat{\mathbf{n}}$ reorients in order to minimize the magnetic free energy. If the field is much larger than a critical field, the system is suddenly placed far from equilibrium. It responds by creating a distortion which maximizes the rate at which the LC lowers its total free energy. This may be a periodic response and the exact form of deformation depends on viscous and elastic coefficients, magnetic field strength, boundary conditions and geometry of the sample. Periodic structures have been found for all classes of nematics.[10–23] The first theoretical study was carried out by Guyon, Meyer, and Salan (GMS) who used nematodynamic equations linearized with respect to the distortion angle. Linear analysis assumes that all modes of distortion are independent and that the only mode which is macroscopically observable is the one with the fastest growth rate. The subsequent application of the GMS approach has been successful in a qualitative sense; that is, given a reasonable estimate for material parameters, the wavelength of a distortion as a function of applied magnetic field is well described by the theory. But the important question of whether the simple analysis of periodic transitions can be refined to a routine for measuring viscous and elastic coefficients has not been resolved.

We report here the results of the first quantitative test of the validity of the linearized theory in the twist geometry. The director $\hat{\mathbf{n}}$ in this geometry is initially aligned parallel to the boundaries and a magnetic field is applied normal to $\hat{\mathbf{n}}$, and in the plane of a sample (Fig. 1). The key factor which enabled us to pursue a quantitatively reliable analysis is that the experiments were performed with the same sealed samples for which the material parameters, shown in Table I, were previously obtained from quasielastic Rayleigh light scattering and field effect measurements.[24]

The particular liquid crystalline system studied was poly-γ-benzyl-glutamate (PBG, from Sigma Chemical Company) in a solvent mixture of methylene chloride and dioxane.[25] Samples were prepared with volume fractions of PBG of 15.5%, 17.1%, and 21.1%. The parallel alignment was achieved by combining oblique evaporation of silicon monoxide and deposition of plasma-polymerized ethylene gas. The detailed description of this technique is reported elsewhere.[26] The lowest magnetic field applied was 5 kG, the highest 12 kG. The instability, when viewed through a microscope with crossed polarizers, appears as a set of stripes perpendicular to the unperturbed director $\hat{\mathbf{n}}_0$ (Fig. 2).

The physical origin for a periodic response is twofold: strong coupling between fluid flow and director rotation, and the large viscous and elastic anisotropy of the nematic phase. More specifically, in a periodic distortion the associated effective viscosity is greatly reduced, and consequently the response speed increased, compared to a uniform distortion involving a large rotational viscosity

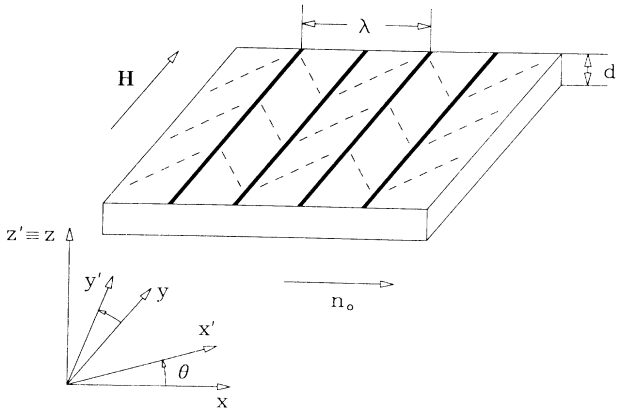

FIG. 1. Geometry of the periodic twist instability. The magnetic field **H** is applied along the y axis to a liquid crystal initially aligned along the x axis. The wavelength of the instability is λ and the thickness of the sample is d. The director $\hat{\mathbf{n}}$ in the mid-plane ($z=0$) is schematically represented by dashed lines. The local (prime) coordinate system is also shown.

TABLE I. Elastic constants and viscosities of PBG used in the numerical integration. All the material parameters (except the elongational viscosity ν_1) were obtained by combining light scattering and field effect measurements (Ref. 24). The value for ν_1 was estimated according to an existing hard rod theory (Ref. 31) and independent experiments on the dynamics of the splay-bend Frederiks transition (Ref. 32). Magnetic susceptibility $\chi_a = 7.19 \times 10^{-9}$ emu/mol for our sample was determined from published x-ray diffraction measurements of the order parameter in nematic PBG.[33]

K_1	K_2 (10^{-7} dyn)	K_3	η_a	η_b	η_c (P)	γ_1	ν_1
12.1	0.78	7.63	1.74	0.37	69.4	69.4	15.0

γ_1. Thus the small wavelengths are favored by dissipation, but on the other hand opposed by elasticity, because large director gradients increase the elastic energy. The optimal wavelength is found to be a balance among drag, elastic, and field forces.

The following discussion refers to one sample only (volume fraction 17.1%, thickness $d = 46.2$ μm), as our results were reproduced by the other two as well. The sample was left in the field until the stripes were well developed and then transferred to a microscope. An attached video camera, interfaced to a computer, was used to digitally record the stripes. The wavelength of the distortion λ, defined as in Fig. 1, was obtained by calculating the intensity autocorrelation function of the image and fitting it to a linearly decaying cosine function. This way the average λ over the entire sample was determined. For each magnetic field strength several measurements were taken. The observed wave vectors $(k_x/k_z)^2$, where $k_x = 2\pi/\lambda$ and $k_z = \pi/d$, were plotted against the growth rate s computed from the linear theory[15] (shown in Fig. 3). Clearly, two conclusions can be deduced from Fig. 3: first, the measured wavelengths significantly differ from the theoretical predictions, and second, they were always shifted towards larger values. We postulated that the systematic offset may be the consequence of nonlinear effects, pronounced at large deformations, where the interaction among different modes can change the finally selected wavelength. Also, material parameters such as the splay elastic constant K_1, elongational flow viscosity ν_1, and shear viscosity η_b, absent in the linearized picture, may be important for the quantitative understanding of the instability at finite amplitude.

To simplify the algebra, the equations of motion are solved in a local coordinate system $(x',y',z' \equiv z)$ attached to the director $(\hat{\mathbf{n}} = \hat{x}')$ and then transformed back to the laboratory reference frame (x,y,z) (shown in Fig. 1). In the prime system the distortion is small; therefore second-order terms in the distortion amplitude can be omitted. We let the initial director $\hat{\mathbf{n}}_0$ be along the x axis and the field $\mathbf{H}$ along the y axis (Fig. 1). The instantaneous director orientation relative to the x axis is defined as $\theta(\mathbf{r},t)$. The director, velocity, and magnetic fields in the laboratory system are

$$\hat{\mathbf{n}} = (\cos\theta, \sin\theta, 0) ,$$
$$\mathbf{v} = (0, v, 0) , \quad (1)$$
$$\mathbf{H} = (0, H, 0) ,$$

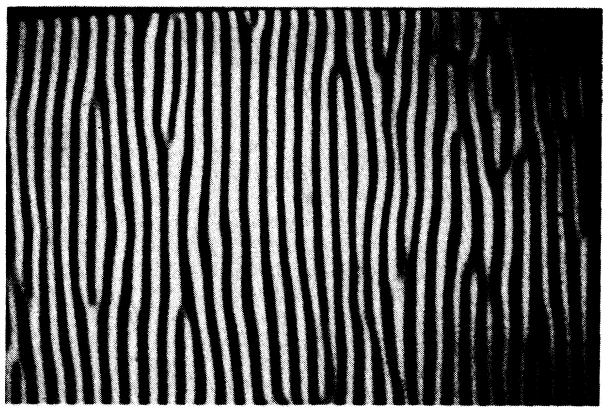

FIG. 2. Polarized photomicrograph of the twist periodic structures in PBG. The magnetic field $H = 10$ kG was applied in the plane of the sample (in the direction of the short edge of the photograph). The average distance between adjacent stripes (half wavelength) is 77.2 μm. The sample thickness $d = 46.2$ μm.

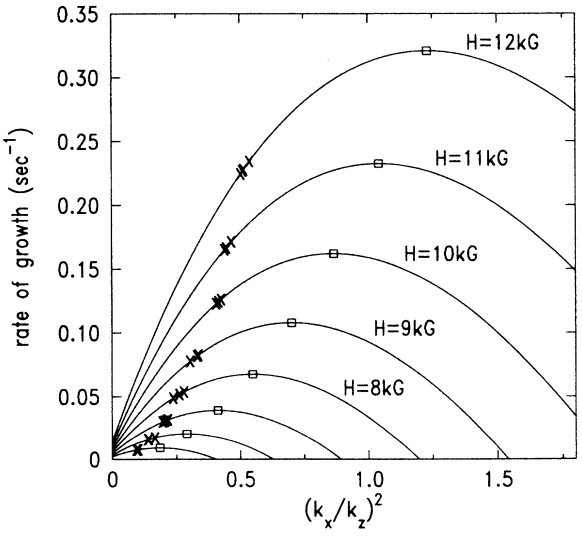

FIG. 3. Rate of growth for different wave vectors. Measured wave vectors (×) vs wave vectors calculated from the linear theory (□) for various field strengths and viscous and elastic coefficients shown in Table I. Calculated wave vectors correspond to the maximum growth rate, drawn with the solid line.

and the transformation of coordinates yields

$$\hat{\mathbf{n}}'=(1,\delta\theta,0)\equiv(1,n_{y'},0)\ ,$$
$$\mathbf{v}'=(v\sin\theta,v\cos\theta,0)\equiv(v_{x'},v_{y'},0)\ , \tag{2}$$
$$\mathbf{H}'=(H\sin\theta,H\cos\theta,0)\equiv(H_{x'},H_{y'},0)\ .$$

Ignoring inertial terms, the balance-of-force equations are

$$0=-\partial_{x'}p+\alpha_3\partial_t\partial_{y'}n_{y'}+2\nu_1\partial_{x'}^2v_{x'}+\eta_4\partial_{x'}\partial_{y'}v_{y'}+\eta_b(\partial_{y'}^2v_{x'}+\partial_{z'}^2v_{x'})\ , \tag{3}$$

$$0=-\partial_{y'}p+\alpha_2\partial_t\partial_{x'}n_{y'}+\eta_c\partial_{x'}^2v_{y'}+\eta_4\partial_{x'}\partial_{y'}v_{x'}+\eta_a(\partial_{z'}^2v_{y'}+2\partial_{y'}^2v_{y'})\ , \tag{4}$$

where p is the pressure, and the five basic viscosities are taken to be the Miesowicz shear viscosities η_a, η_b, and η_c, along with elongational flow viscosity ν_1 and pure rotational viscosity γ_1. The coupling viscosities are $\alpha_2=\frac{1}{2}(\eta_b-\eta_c-\gamma_1)$, $\alpha_3=\frac{1}{2}(\eta_b-\eta_c+\gamma_1)$, and $\eta_4=\frac{1}{2}(\eta_b+\eta_c-\gamma_1)$.

The balance-of-torque equation is

$$\gamma_1\partial_t n_{y'}=-\alpha_2\partial_{x'}v_{y'}-\alpha_3\partial_{y'}v_{x'}+K_1\partial_{y'}^2n_{y'}+K_2\partial_{z'}^2n_{y'}+K_3\partial_{x'}^2n_{y'}+\chi_a(H_{x'}H_{y'}+H_{y'}^2n_{y'})\ , \tag{5}$$

where χ_a is the anisotropy of the susceptibility and K_1, K_2, and K_3 are the splay, twist, and bend elastic constants, respectively.

After transforming Eqs. (3)–(5) to the laboratory system and eliminating pressure from (3) and (4), we are left with

$$\partial_t\partial_x\theta(\alpha_3\sin^2\theta-\alpha_2\cos^2\theta)=\partial_x^2v[2(\nu_1-\eta_4+\eta_a)\sin^2\theta\cos^2\theta+\eta_c\cos^4\theta+\eta_b\sin^4\theta]+\partial_z^2v(\eta_a\cos^2\theta+\eta_b\sin^2\theta)\ , \tag{6}$$

$$\gamma_1\partial_t\theta=\partial_xv(\alpha_3\sin^2\theta-\alpha_2\cos^2\theta)+\partial_x^2\theta(K_1\sin^2\theta+K_3\cos^2\theta)+K_2\partial_z^2\theta+\chi_aH^2\sin\theta\cos\theta\ . \tag{7}$$

Equations (6) and (7) are solved numerically in the mid-plane ($z=0$) (Fig. 1) assuming a harmonic dependence along the z axis for both director and velocity

$$\theta=\theta(x,t)\cos(z\pi/d)\ ,$$
$$v=v(x,t)\cos(z\pi/d)\ . \tag{8}$$

The test of the plausibility of this assumption is described further below.

The numerical integration was carried out on a grid consisting of 256 points using a forward finite difference method.[27,28] This differencing scheme was checked against a more sophisticated *fully implicit*[28] method, but it turned out to perform equally well. The sample length L was chosen to accommodate approximately the same number of wavelengths as the real sample. Fixed boundary conditions were used, $\theta(0,t)=\theta(256,t)=0$ and $v(0,t)=v(256,t)=0$, reflecting the actual physical situation. For each computer run a random initial condition, in which different Fourier components of the director were properly weighted by a Boltzmann factor, was created in a standard way.[29,30] To be more specific, we briefly describe the procedure. The Fourier decomposed free energy of the orientational fluctuations can be written as

$$F_q=\frac{1}{2V}\sum_q|A_q|^2(K_3q_x^2+K_2q_z^2)\ , \tag{9}$$

where $A(q)$ is the amplitude of the corresponding Fourier mode, V is the volume, and $q_z=\pi/d$ (d is the sample thickness). In our case $q_x=(\pi/L)n$, $n=1,2,\ldots,256$ is a quantized wave vector, and $V=L^2d$. By applying the equipartition theorem to Eq. (9), the thermally averaged expectation value of the amplitude of the director fluctuation (per normal mode) can be expressed as

$$\langle|A(q)|^2\rangle=\frac{k_BT}{V(K_3q_x^2+K_2q_z^2)}\ , \tag{10}$$

where k_B is the Boltzmann constant and T is the temperature.

There are 256 $\theta(x,0)$ values, and each of them is represented by the sum of 256 Fourier modes. For example, the x_lth element is

$$\theta(x_l,0)=\sum_{j=1}^{256}A_j\sin(q_jx_l+\phi)\ , \tag{11}$$

where ϕ is the random phase constrained to be either π or 0 because of fixed boundary conditions. For each q_j mode, a familiar Monte Carlo scheme is then employed to select a random set of initial amplitudes A_j, which conform to the distribution function of Eq. (10).

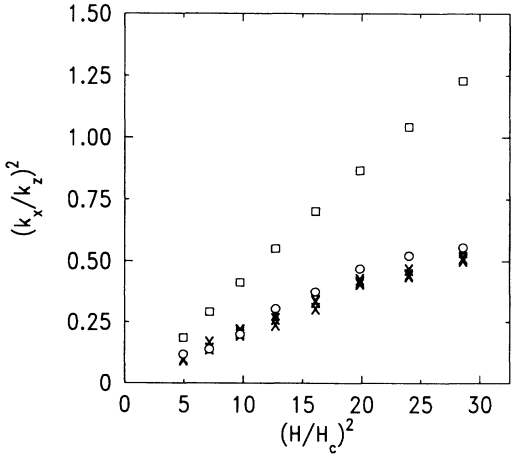

FIG. 4. Comparison between measured wave vectors and wave vectors obtained from the numerical integration as a function of magnetic field strength. Experimental values (×), numerical calculation (○), and the linear theory (□). The twist critical field $H_c=2.24$ kG.

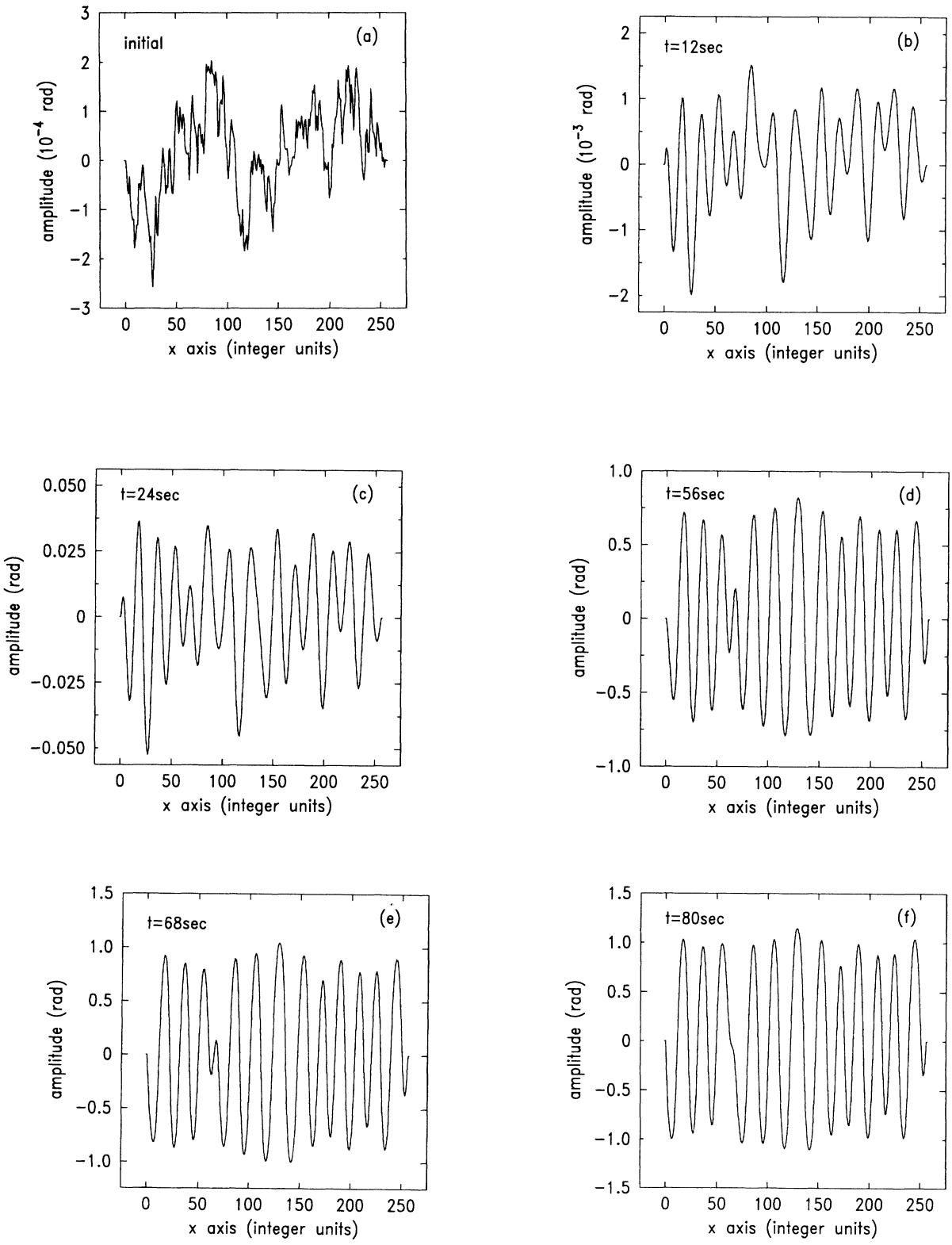

FIG. 5. An example of the numerical integration showing the real-space time evolution of $\theta(x,t)$. From a random initial condition with an amplitude of 10^{-4} rad (a), a regular pattern emerges with the periodicity well described by the linearized model (b) and (c). As the distortion grows, parts of the initial periodicity disappear (d) and (e), thus increasing the final average wavelength (f). The distance between two consecutive points in the integer scale corresponds to 8.5 μm real scale.

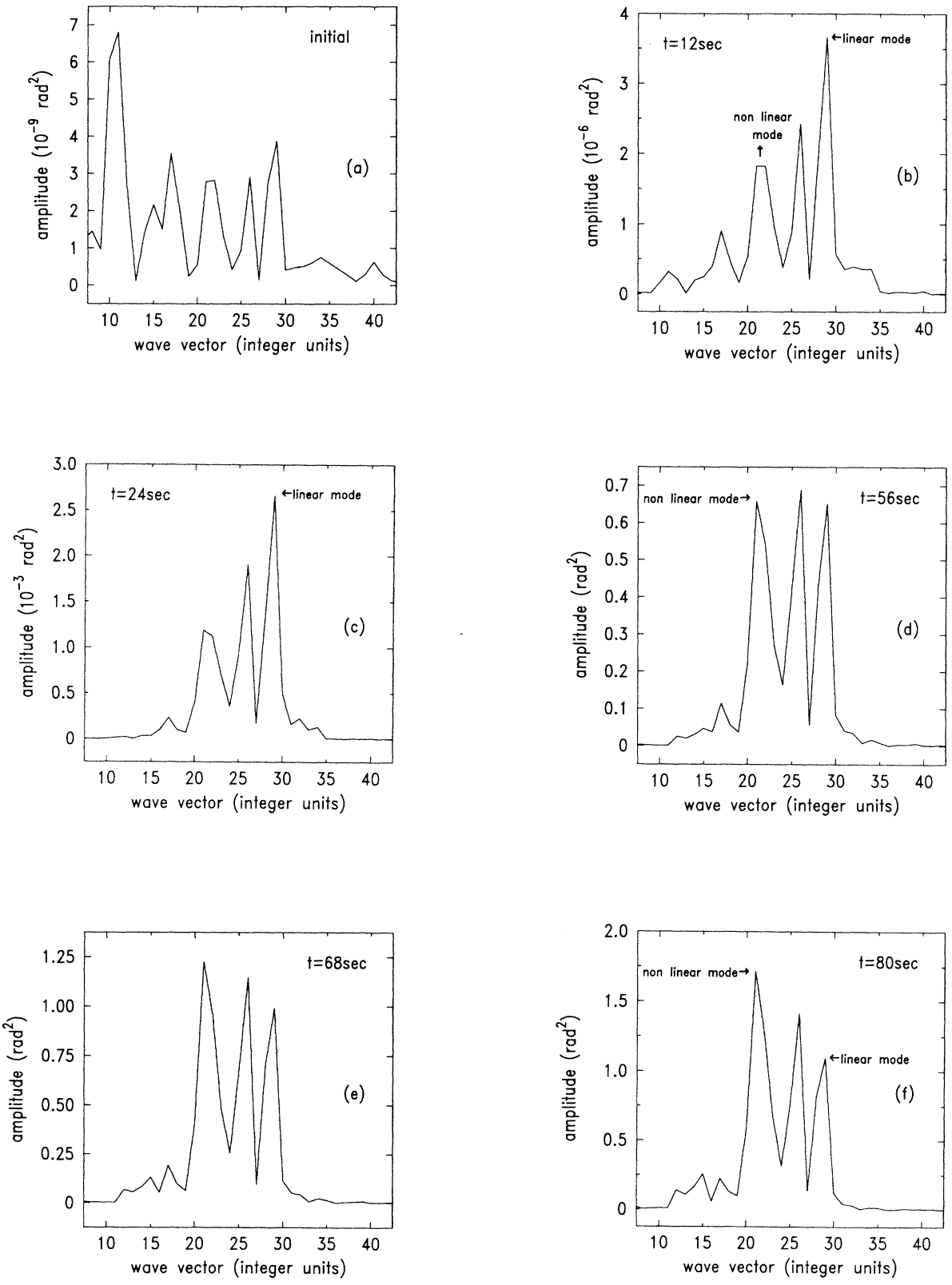

FIG. 6. Power-spectrum evolution of a band of wave vectors corresponding to Fig. 5. Starting from thermally weighted random initial condition (a), two regimes can be distinguished. At early times the fastest growing distortion mode is the one calculated from the linearized theory (b) and (c). At later times a mode with a smaller wave vector, or equivalently longer wavelength grows the fastest (d) and (e). The final wavelength is shifted towards longer values (f).

The magnetic field dependence of the wave vectors for the experimental data, linear theory, and our numerical integration is shown in Fig. 4. The numerical result for each field is an average over ten runs. Obviously, the nonlinear calculation reproduced the measurements to a high degree of accuracy. The small discrepancy may be attributed to the neglect of the nonlinearities along the z direction. We numerically investigated this possibility by assuming now that the wavelengths along the x direction are adequately described by the linear theory and we calculated the director along z. For large angles of distortion, as expected, we found deviations from a cosine function. However, the final wavelength selection has already occurred by that time, so the implementation of the two-dimensional model would not contribute much further physical insight into the instability.

To understand why the observed wavelengths differ from ones predicted by the linear theory we have studied the amplitude evolution for both $\theta(x,t)$ and $v(x,t)$. This is easily achieved by Fourier transforming $\theta(x,t)$ to $\theta(k,t)$ and $v(x,t)$ to $v(k,t)$, and monitoring the corresponding power spectrum $|\theta(k,t)|^2$ and $|v(k,t)|^2$. Examples of how $\theta(x,t)$ and its power spectrum $|\theta(k,t)|^2$ for a band of wave vectors change in time are shown in Figs. 5 and 6, respectively. This particular sequence was accomplished with the amplitude of the initial state of the order of 10^{-4} rad, field strength of $H=8$ kG, and viscous and elastic coefficients given in Table I. For small amplitudes the fastest growing distortion mode is indeed the one calculated from the linear theory. But as the deformation becomes larger, the linear mode slows down and a mode with a smaller wave vector starts to grow faster, shifting the observed average wavelength to larger values. The essential features of Fig. 6 were reproduced for other fields as well.

Once the field has been applied, the selected wavelength depends on both the viscosities and the elasticities. But their relative influence may differ at various stages of evolution. Initially, the fluid velocity changes significantly, indicating the greater impact of the viscosities at early times. As the distortion continues to grow, the velocity starts to decrease, which means that the elasticities begin dominating the process. They tend to eliminate large director gradients by forcing the wavelength to be as long as possible.

To test this idea we plotted the power-spectrum evolution of $\theta(k,t)$ [Fig. 7(a)] and $v(k,t)$ [Fig. 7(b)], as a function of time for two wave vectors; the fastest one as calculated from the linear theory and the other which had the final maximum amplitude. We call this latter a *nonlinear* mode. By comparing Figs. 7(a) and 7(b), at the time interval when the *nonlinear* mode takes over [Fig. 7(a)], the velocity [Fig. 7(b)] has dropped by a factor of 3 from its maximum value. This is in agreement with our model. Further evidence that the energetics plays an important role comes from the study of the impact of material constants on the selected wavelengths. Although there are no free parameters in the numerical integration, by varying elastic and viscous coefficients absent in the linear theory (K_1, η_b, and ν_1), we observed that only the splay elastic constant K_1 significantly affected the wavelengths. Increasing K_1 by 25% would increase λ by about 10%. On the other hand, changing both η_b and ν_1 by a factor of 2, made essentially no impact ($<1\%$) on wavelength.

The proposed model of two distinct stages in the evolution of the periodic twist instability, initially dominated by viscosities and finally by elasticities, motivates further challenging investigations. For example, experimental verification requires measurements of both amplitude of the distortion and velocity of the fluid as a function of time, and requires comparing them with values obtained from the equations of motion. Furthermore, in the absence of a general theory, one can try to develop models based on this work which describe interaction among competing nonlinear modes.

To conclude, we derived nonlinear equations of

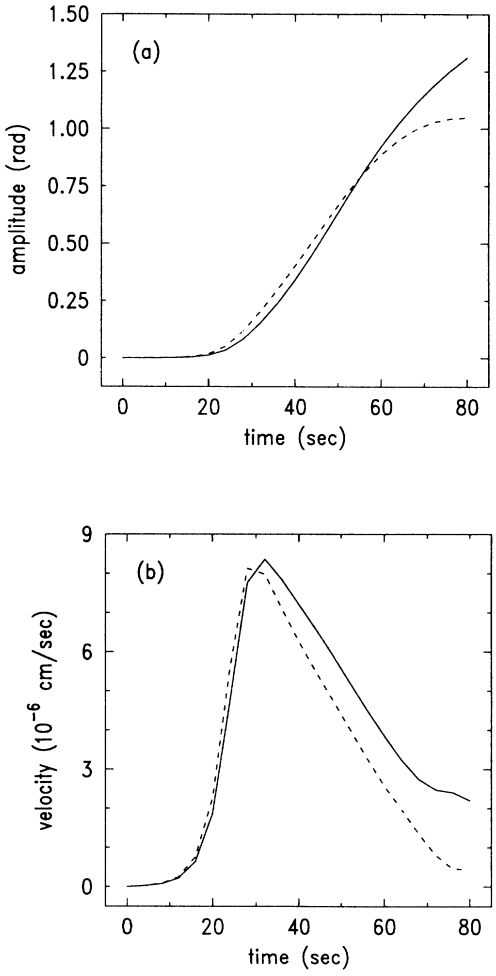

FIG. 7. (a) The square root of the power-spectrum evolution of *linear* (— — —) and *nonlinear* (——) distortion modes. Initially the *linear* mode is faster. At deformations $\theta > \pi/4$; the amplitude of the *nonlinear* mode exceeds the *linear* mode. (b) The same as (a) for the velocity. The *nonlinear* mode of (a) takes over at the point where the velocity (b) has decreased by a factor of 3.

motion, the solution of which accurately fitted the experimental data. In turn, this means that the linear theory is inadequate for extracting ratios of material parameters from the twist periodic Frederiks transition. The nonlinear calculation may be applicable, but only if the number of unknown constants is limited to two or three. Otherwise, one can always find a consistent set of eight parameters to fit this model without knowing whether the values obtained are unique. The splay elastic constant is an important parameter at large distortions. And finally, we proposed a novel mechanism responsible for the observed wavelength selection.

We gratefully acknowledge useful discussions with Frank Lonberg, Sindoo Lee, Leigh Sneddon, Takashi Odagaki, Henk Lekkerkerker, Walter Zimmermann, and Lorenz Kramer. This research was supported in part by the National Science Foundation through Grant No. DMR-8803582 and by the Martin Fisher School of Physics, Brandeis University.

---

*Present address: AT&T Bell Laboratories, 600 Mountain Avenue, Murray Hill, NJ 07974-2070.

†Present address: Max-Planck-Institute, Hochfeld Magnetlabor, 38042 Grenoble, France.

[1]L. Kramer, E. Ben-Jacob, H. Brandt, and M. C. Cross, Phys. Rev. Lett. **49**, 1891 (1982).

[2]G. Dee and J. S. Langer, Phys. Rev. Lett. **50**, 383 (1985).

[3]W. van Saarloos, Phys. Rev. Lett. **58**, 2571 (1987).

[4]W. van Saarloos, Phys. Rev. A **37**, 211 (1988).

[5]E. L. Koschmieder, Adv. Chem. Phys. **32**, 109 (1975).

[6]J. P. Gollub, in *Nonlinear Dynamics and Turbulence,* edited by G. I. Barenblatt, G. Iooss, and D. D. Joseph (Pitman, New York, 1983).

[7]F. H. Busse, in *Hydrodynamic Instabilities and the Transition to Turbulence,* edited by H. L. Swinney (Springer-Verlag, Berlin, 1981).

[8]J. S. Langer, Rev. Mod. Phys. **52**, 1 (1980).

[9]D. Feinn, P. Ortoleva, W. Scalf, S. Schmidt, and M. Wolff, J. Chem. Phys. **69**, 27 (1978).

[10]E. F. Carr, Mol. Cryst. Liq. Cryst. **34**, L159 (1977).

[11]E. Guyon, R. Meyer, and J. Salan, Mol. Cryst. Liq. Cryst. **54**, 261 (1979).

[12]J. Charvolin and Y. Hendrikx, J. Phys. (Paris) Lett. **41**, L597 (1980).

[13]L. J. Yu and A. Saupe, J. Am. Chem. Soc. **102**, 4879 (1980).

[14]H. Lee and M. M. Labes, Mol. Cryst. Liq. Cryst. **84**, 137 (1982).

[15]F. Lonberg, S. Fraden, A. J. Hurd, and R. B. Meyer, Phys. Rev. Lett. **52**, 1903 (1984).

[16]A. J. Hurd, S. Fraden, F. Lonberg, and R. B. Meyer, J. Phys. (Paris) **46**, 905 (1985).

[17]S. Fraden, A. J. Hurd, R. B. Meyer, M. Cahoon, and D. L. D. Caspar, J. Phys. (Paris) Colloq. **46**, C3-85 (1985).

[18]Y. W. Hui, M. R. Kuzma, M. San Miguel, and M. M. Labes, J. Chem. Phys. **83**, 288 (1985).

[19]D. V. Rose and M. R. Kuzma, Mol. Cryst. Liq. Cryst. **4**, L39 (1986).

[20]M. R. Kuzma, Phys. Rev. Lett. **57**, 349 (1986).

[21]C. R. Fincher, Jr., Macromolecules **19**, 2431 (1986).

[22]A. F. Martins, P. Esnault, and F. Volino, Phys. Rev. Lett. **57**, 1745 (1986).

[23]J. P.McClymer and M. M. Labes, Mol. Cryst. Liq. Cryst. **144**, 275 (1987).

[24]V. G. Taratuta, F. Lonberg, and R. B. Meyer (private communication).

[25]Conmar Robinson, Tetrahedron **13**, 219 (1961).

[26]V. G. Taratuta, G. M. Srajer, and R. B. Meyer, Mol. Cryst. Liq. Cryst. **116**, 245 (1985).

[27]J. H. Ferziger, *Numerical Methods for Engineering Application* (Wiley, New York, 1981).

[28]W. H. Press, B. P. Flannery, S. Teukolsky, and W. T. Vetterling, *Numerical Recipes* (Cambridge University Press, Cambridge, England, 1985).

[29]N. Metropolis, A. W. Rosenbluth, M. N. Rosenbluth, A. H. Teller, and E. Teller, J. Chem. Phys. **21**, 1087 (1953).

[30]K. Binder, in *Application of the Monte Carlo Method in Statistical Physics,* edited by K. Binder (Springer-Verlag, Berlin, 1984).

[31]S.-D. Lee and R. B. Meyer, J. Chem. Phys. **84**, 3443 (1986).

[32]F. Lonberg (private communication).

[33]N. S. Murthy, J. R. Knox, and E. T. Samulski, J. Chem. Phys. **65**, 4835 (1976).

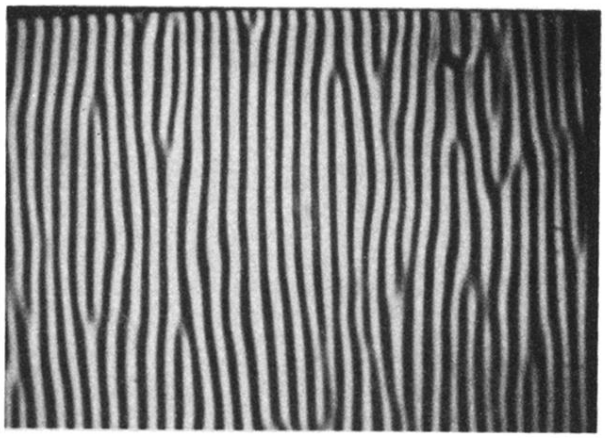

FIG. 2. Polarized photomicrograph of the twist periodic structures in PBG. The magnetic field $H = 10$ kG was applied in the plane of the sample (in the direction of the short edge of the photograph). The average distance between adjacent stripes (half wavelength) is 77.2 μm. The sample thickness $d = 46.2$ μm.